Optics Letters

Highly flexible organic–inorganic hybrid perovskite light-emitting devices based on an ultrathin Au electrode

Yu-Shan Liu,[1] Shuang Guo,[1] Fang-Shun Yi,[1] Jing Feng,[1,3] and Hong-Bo Sun[1,2,4]

[1]State Key Laboratory of Integrated Optoelectronics, College of Electronic Science and Engineering, Jilin University, Changchun 130012, China
[2]State Key Laboratory of Precision Measurement Technology and Instruments, Department of Precision Instrument, Tsinghua University, Haidian, Beijing 100084, China
[3]e-mail: jingfeng@jlu.edu.cn
[4]e-mail: hbsun@tsinghua.edu.cn

Received 22 August 2018; accepted 5 October 2018; posted 12 October 2018 (Doc. ID 342988); published 5 November 2018

Organic–inorganic hybrid perovskite materials have received much attention in light-emitting applications during the past several years. The commonly used indium tin oxide (ITO) electrodes in perovskite light-emitting devices (PeLEDs) have unavoidable drawbacks of increasing cost and incompatibility with flexible devices, which limit the development of PeLEDs. Here, high-performance and ITO-free flexible PeLEDs utilizing ultrathin Au electrodes have been achieved and exhibited high brightness ($>10,000$ cdm^{-2}). By introducing a MoO_3/SU-8 modification layer, the ultrathin Au film with a thickness of 7 nm exhibits excellent surface morphology with a root-mean-square roughness value of 0.307 nm. Meanwhile, the ultrathin Au film demonstrates an outstanding optical property with transparency of 83% at the wavelength of 550 nm. Simultaneously, favorable conductivity with a sheet resistance of 13 Ω sq^{-1} has been achieved. High mechanical robustness and flexibility have been obtained for the flexible PeLEDs by surviving 1000 bending cycles. The flexible PeLEDs reported here exhibit tremendous potential for commercial applications.

https://doi.org/10.1364/OL.43.005524

Organic–inorganic hybrid perovskite materials have achieved substantial progress over recent years due to the characteristics of both organic materials and inorganic materials, such as low material cost, long carrier diffusion lengths, ambipolar carrier transport, tunable band gap, and easy fabrication [1–5]. Recently, perovskite light-emitting devices (PeLEDs) using $MAPbBr_3$ as the emitting layer have achieved high electroluminescence (EL) performance at room temperature [6–10]. Qasim *et al.* also reported high-performance multicolor PeLEDs fabricated using an all-solution process [11]. However, very few flexible PeLEDs have been reported, since most devices were fabricated using indium tin oxide (ITO) electrodes, which have many drawbacks such as fragile properties and difficulty in the fabricating process [12,13]. Therefore, new kinds of transparent electrodes are in urgent need to replace the ITO film. Alternative conductive transparent electrodes have been reported in flexible PeLEDs, such as polymer conductors [14,15], silver nanowires [16,17], and graphene films [18–20]. Ultrathin metallic films with excellent transmittance and conductivity have been employed in perovskite solar cell devices to replace ITO [21–23], which indicates its potential as the transparent electrode in PeLEDs.

Here, high-performance and ITO-free flexible organic–inorganic hybrid PeLEDs have been demonstrated by utilizing an ultrathin Au electrode. The ultrathin Au film with a thickness of 7 nm was deposited on a SU-8 modified substrate with a seed layer of MoO_3. The 7-nm ultrathin Au film exhibits an excellent surface morphology, outstanding optical properties, and favorable conductivity, which is comparable to that of ITO. Higher device efficiency has been obtained after replacing ITO with the ultrathin Au electrode. The flexible PeLEDs based on the ultrathin Au electrode exhibited high brightness of 11270 cd/m^2 and outstanding mechanical stability of over 1000 bending cycles.

The structure of the PeLEDs was Glass/SU-8/MoO_3/ultrathin Au/PEDOT: PSS (100 nm)/$MaPbBr_3$ (150 nm)/TPBi (35 nm)/LiF (1 nm)/Al (100 nm) [Fig. 1(a)]. The components of the devices were carefully deposited, and its layered structure can be confirmed in the cross-sectional image obtained with a scanning electron microscope (SEM) [Fig. 1(b)]. The work function of Au (5.1 ev) is higher than that of ITO (4.7 ev). Therefore, a lower hole injection barrier from the anode to the hole injection layer (HIL) can be obtained by using the ultrathin Au electrode. Furthermore, in the case of ITO-based devices, ITO can contaminate the HIL, because In and Sn atoms can be released and diffuse from ITO to the upper layers during the formation of HIL. The diffused atoms form interfacial trap states, which results in decreased hole-injection efficiency of the HIL [7,24]. In contrast, Au atoms are more chemically stable, meaning that these phenomena are less likely to happen.

As an option of the transparent anode in PeLEDs, the surface morphology of electrode film is of great importance, since

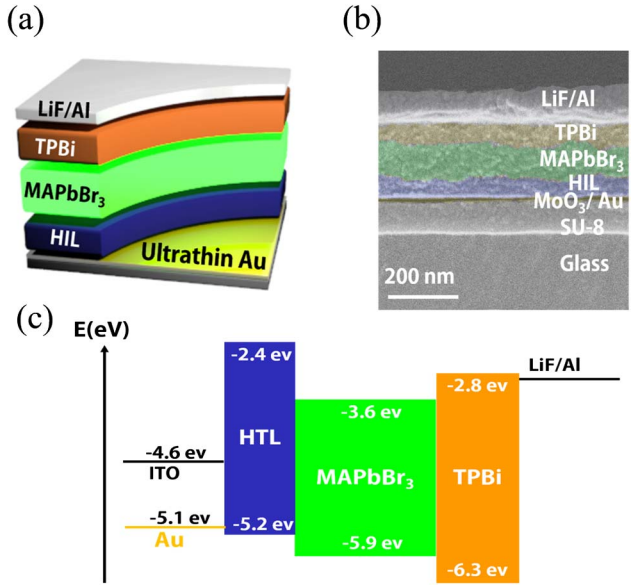

Fig. 1. (a) Schematic device structure of PeLED with ultrathin Au electrode and $MAPbBr_3$ emitter. (b) Cross-sectional SEM image of the PeLED. (c) Energy band structure of PeLED with Au or ITO electrodes.

the device performance was affected by surface smoothness. The quality of the metallic film (continuity, conductivity, transmittance, etc.) was governed by the nucleation process and growth kinetics, which is strongly associated with the substrate [25]. The surface morphology of Au film on the glass substrate, SU-8 modified substrate, and MoO_3/SU-8 modified substrate are investigated by SEM and shown in Fig. 2. Because of the various bonding energies between Au and the substrate caused by different surface energies, thermally evaporated metallic atoms on differing substrates normally leads to surface energy mismatch in different extents between metallic films and corresponding substrates [16]. As shown in Fig. 2(a), the Au film deposited directly on the glass substrate exhibits a distinct three-dimensional island growth mode, which causes large cracks and high roughness (Ra = 0.776 nm), while Au films on SU-8 modified substrate [Fig. 2(b)] and MoO_3/SU-8 modified substrate [Fig. 2(c)] exhibit decreasing surface cracks and roughness (Ra = 0.581 – 0.307 nm). This significant improvement in surface smoothness is attributed to strong chemical covalent bonds between the SU-8 layer and Au atoms [16]. More importantly, the MoO_3 seed layer could further enhance nucleation sites and suppress surface diffusion of metallic atoms, thereby forming an ultrathin and smooth Au transparent electrode film [13].

Improved continuity and surface morphology of the metallic film would enhance the conductivity and transmittance of Au

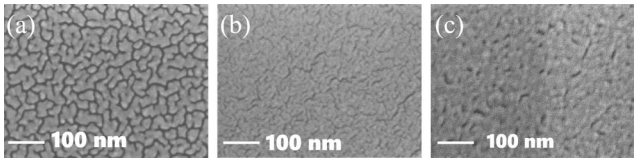

Fig. 2. SEM image of surface morphologies of the 7-nm ultrathin Au film deposited on bare glass substrate (a), on SU-8 modified glass substrate (b), and on MoO_3/SU-8 modified glass substrate (c).

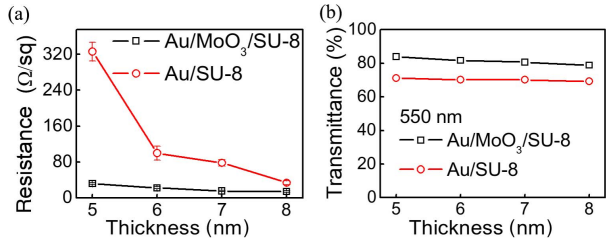

Fig. 3. (a) Sheet resistance (Rs) of the Au/SU-8 and Au/MoO_3/SU-8 films as the function of Au film thickness. (b) Transmittance of the Au/SU-8 and Au/MoO_3/SU-8 films as the function of Au film thickness at the wavelength of 550 nm.

film effectively. Figure 3 shows the square resistance (Rs) and transmittance of the Au film with bare and modified glass substrates. As shown in Fig. 3(a), the Au film deposited on MoO_3/SU-8 modified substrate exhibits apparently lower Rs than that of Au on only SU-8 modified substrate due to the MoO_3-induced uniform and continuous Au film deposition. The 5-nm Au film on MoO_3/SU-8 modified substrate has a Rs of approximately 35 Ω/sq, while, the Au film on SU-8 modified substrate with the same thickness has a nearly 10-times higher Rs (320 Ω/sq). With the thickness of Au increasing to 8 nm, the Rs of the Au film on SU-8 modified substrate declined to 30 Ω/sq. It is two times higher than that of the Au/MoO_3/SU-8 film (12 Ω/sq) with the same thickness, and comparable to the conductivity of ITO films (10 Ω/sq). On the contrary, Au film deposited directly on a glass substrate remains insulative until the thickness is over 10 nm, indicating that the modified substrate has an obvious effect on improving the electronic conductivity of the metallic film. On the other hand, the transmittance of the Au/MoO_3/SU-8 film is increased compared to that of the Au/SU-8 film, as shown in Fig. 3(b). Obviously enhanced transmittance is observed from the Au film deposited on MoO_3/SU-8 modified substrate from 500 nm to 800 nm, which is beneficial to the green-color PeLEDs.

It is well known that the crystallization quality of $MAPbBr_3$ film is the key factor to fabricate high-performance light-emitting devices. The PeLED with an untreated $MAPbBr_3$ layer had low performance because of the poor quality of crystallization of the $MAPbBr_3$ emitting layer. As shown in Fig. 4(a), $MAPbBr_3$ film annealed at 95°C without treatment resulted in smaller grain size of the perovskite microcrystal, which leads to larger specific surface area of the crystalline grain. The increasing number in surface defects and traps generates more non-radiative recombination. Therefore, we use a solvent-vapor annealing treatment to enhance the quality of the $MAPbBr_3$ emitting layer. The $MAPbBr_3$ film annealed using a solvent-vapor annealing treatment [Fig. 4(b)] exhibits a larger size of microcrystal grain, indicating that the $MAPbBr_3$ microcrystal grain continued growing in the N,N-Dimethylformamide (DMF) atmosphere for a short while and further enhanced crystallization quality. From the X-ray diffraction (XRD) pattern in Fig. 4(c), we can see that no obvious impure peaks can be observed. The grain size has been improved, as the peak area of solvent-vapor-annealed $MAPbBr_3$ film is larger (area = 2788.22) than that of the untreated $MAPbBr_3$ film (area = 1537.42). Figure 4(d) shows the absorption of the $MAPbBr_3$ film without

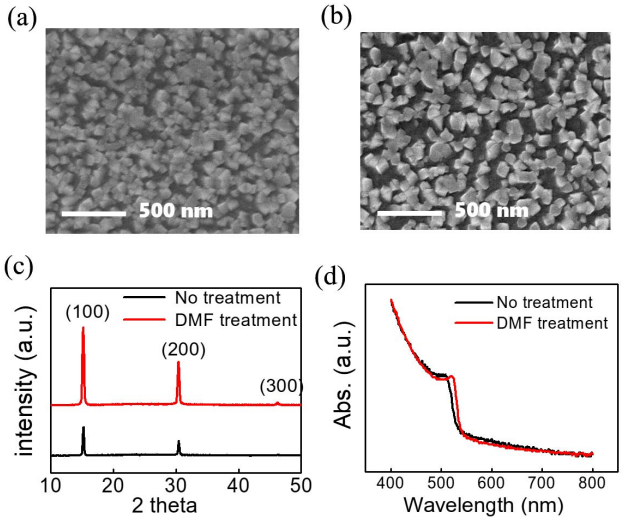

Fig. 4. Characterization of the $MAPbBr_3$ films. SEM images of $MAPbBr_3$ films without (a) and with (b) solvent-vapor annealing treatment. X-ray diffraction (XRD) (c) and absorption (d) patterns of $MAPbBr_3$ films without and with solvent-vapor annealing treatment.

and with the solvent-vapor annealing treatment. A slight red shift of the absorption edge is observed after the $MAPbBr_3$ film is treated in DMF solvent-vapor annealing, while no other absorption peak appears, indicating that the solvent-vapor annealing process did not influence the crystalline purity of the $MAPbBr_3$ microcrystal. We carried out tests of steady-state photoluminescence (PL) [Fig. 5(a)] and PL lifetime [Fig. 5(b)] on $MAPbBr_3$ films under different conditions. The $MAPbBr_3$ films without solvent-vapor treatment showed weak green emission at 496 nm. The $MAPbBr_3$ film with solvent-vapor treatment exhibited a dramatic increase in PL intensity, indicating that non-radiative recombination in the perovskite layer or at the interfaces has been significantly suppressed. We next acquired PL lifetime curves [Fig. 5(b)] of the $MAPbBr_3$ film with and without solvent-vapor treatment. The PL lifetime of the $MAPbBr_3$ film was increased from 11.8 ns to 16.9 ns after DMF solvent-vapor treatment. The enhancement of PL might arise from the assistance of DMF solvent-vapor treatment. With the degree of crystallinity improved, larger grain sizes bring less specific surface area compared to those in the $MAPbBr_3$ film without solvent-vapor treatment. Therefore,

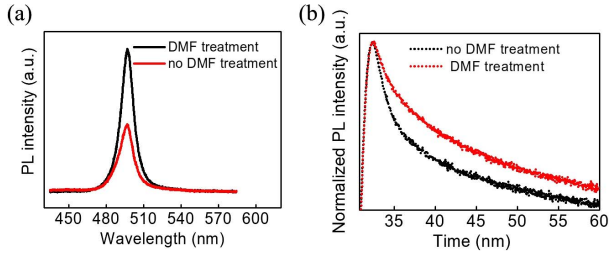

Fig. 5. PL behavior of $MAPbBr_3$ films under different treatment conditions. (a) Steady-state PL of $MAPbBr_3$ films with and without DMF solvent-vapor treatment. (b) PL lifetime measurement of $MAPbBr_3$ films with and without DMF solvent-vapor treatment.

the improved grain size reduced non-radiative recombination at grain boundaries, leading to enhanced PL. It should be noted that we believe it is unbeneficial for the $MAPbBr_3$ film if the solvent-vapor treatment time was too long to make the grain size too large. Constant treatment of solvent-vapor may damage the crystal structure of perovskite, thereby resulting in device performance degradation. Therefore, time of treatment should be controlled strictly to ensure the $MAPbBr_3$ film is of the best quality.

EL performances of PeLEDs with ultrathin Au electrodes are compared with ITO-based devices and shown in Fig. 6. The PeLED with ultrathin Au electrodes exhibit higher device performance as expected, owning to good surface morphologies and optical and electrical characteristics of the ultrathin metallic film. To be specific, the ultrathin Au-electrode PeLED shows maximum luminance (11270 cd/m^2) similar to ITO-electrode PeLED, while the latter one experienced a rapid decrease in the aspect of luminance and current density after 7 V [Fig. 6(a)]. Furthermore, the current efficiency is increased from 2.9 cd/A for the ITO-electrode PeLED to 3.3 cd/A for the Au-electrode PeLED [Fig. 6(b)]. Enhancement of EL performance arises from the excellent characteristics of the ultrathin Au film, as well as suppression of the power loss induced by the waveguide modes associated with the ITO electrode [26]. The modified substrate (MoO_3/SU-8) under an Au anode as a refractive-index-matching layer to improve the light extraction is also beneficial to improve the efficiency of PeLEDs.

Bending tests have been conducted to examine the flexibility and mechanical robustness of the ultrathin Au film and Au-anode-based PeLEDs by using a flexible NOA63 substrate. The fabricating method of the flexible substrate was reported in previous work [22,27,28]. The bending radius was 5 mm, and the thickness of the flexible substrate was 500 μm. The ultrathin Au film showed remarkable mechanical robustness, and its sheet resistance remained almost unchanged after 1000 times repeated bending [Fig. 6(d)]. The luminance of the flexible PeLEDs decreased to 50% of its initial values after 1000 bending cycles [Fig. 6(c)]. The inset is the photograph of the ultrathin Au-based PeLED working at 5 V while being bended.

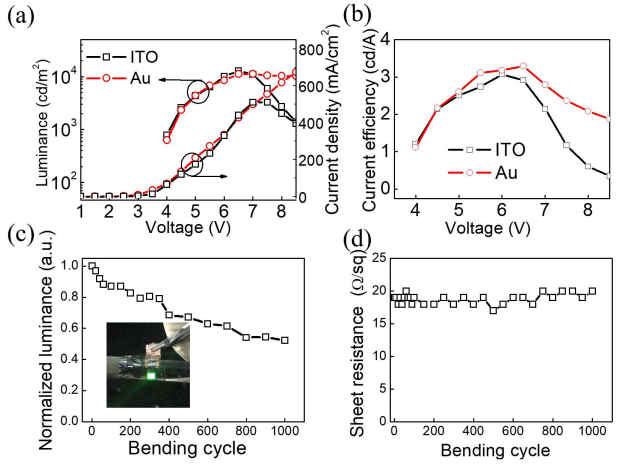

Fig. 6. EL performances of the PeLEDs. Current density-luminance-voltage curves (a), current efficiency-voltage curves of PeLEDs with ITO and ultrathin Au electrodes (b), normalized luminance of flexible PeLEDs based on ultrathin Au anode as a function of bending cycles at a bending radius of 5 mm (c), and sheet resistance as a function of bending cycles (d).

The degradation of the flexible PeLED is mainly because of poor chemical stability of the perovskite material itself [29]. Therefore, it is possible for the flexible PeLEDs to further improve long-time working stability if an optimizing process on enhancing chemical and voltage stability of $MAPbBr_3$ is done.

In summary, we have fabricated ITO-free flexible PeLEDs with ultrathin Au transparent electrodes. The ultrathin Au film with a 7-nm thickness exhibits an ultra-smooth surface, excellent conductivity, and mechanical robustness by introducing the MoO_3/SU-8 modified layer. The RMS roughness and sheet resistance are 0.3 nm and $13\,\Omega\,sq^{-1}$, respectively, and the sheet resistance remains stable after 1000 times repeated bending. By applying the ultrathin Au film as the electrode of the PeLEDs, 10% improved current efficiency compared with the ITO-based devices was realized. High flexibility and mechanical robustness have been demonstrated for ultrathin Au-based PeLEDs, which can continue working after 1000 bending cycles. Properties of the ultrathin Au film satisfy the requirements of flexible transparent electrodes in PeLEDs and provide a simple had highly feasible approach for large-area and flexible PeLEDs.

Funding. National Key Research and Development Program of China (2017YFB0404500); National Natural Science Foundation of China (NSFC) (61825402, 61590930, 61605056, 61675085, 61705075).

REFERENCES

1. H. Cho, S. H. Jeong, M. H. Park, Y. H. Kim, C. Wolf, C. L. Lee, J. H. Heo, A. Sadhanala, N. Myoung, S. Yoo, S. H. Im, R. H. Friend, and T. W. Lee, Science **350**, 1222 (2015).
2. Z. K. Tan, R. S. Moghaddam, M. L. Lai, P. Docampo, R. Higler, F. Deschler, M. Price, A. Sadhanala, L. M. Pazos, D. Credgington, F. Hanusch, T. Bein, H. J. Snaith, and R. H. Friend, Nat. Nanotechnol. **9**, 687 (2014).
3. N. J. Jeon, J. H. Noh, W. S. Yang, Y. C. Kim, S. Ryu, J. Seo, and S. I. Seok, Nature **517**, 476 (2015).
4. X. Zhang, H. Liu, W. Wang, J. Zhang, B. Xu, K. L. Karen, Y. Zheng, S. Liu, S. Chen, K. Wang, and X. W. Sun, Adv. Mater. **29**, 1606405 (2017).
5. F. Guo, A. Karl, Q.-F. Xue, K. C. Tam, K. Forberich, and C. J. Brabec, Light: Sci. Appl. **6**, e17094 (2017).
6. L. Zhao, Y. W. Yeh, N. L. Tran, F. Wu, Z. Xiao, R. A. Kerner, Y. L. Lin, G. D. Scholes, N. Yao, and B. P. Rand, ACS Nano **11**, 3957 (2017).
7. H. K. Seo, H. Kim, J. Lee, M. H. Park, S. H. Jeong, Y. H. Kim, S. J. Kwon, T. H. Han, S. Yoo, and T. W. Lee, Adv. Mater. **29**, 1605587 (2017).
8. L. S. Cui, Y. M. Xie, Y. K. Wang, C. Zhong, Y. L. Deng, X. Y. Liu, Z. Q. Jiang, and L. S. Liao, Adv. Mater. **27**, 4213 (2015).
9. N. K. Kumawat, A. Dey, K. L. Narasimhan, and D. Kabra, ACS Photon. **2**, 349 (2015).
10. H.-W. Chen, R.-D. Zhu, J. He, W. Duan, W. Hu, Y.-Q. Lu, M.-C. Li, S.-L. Lee, Y.-J. Dong, and S.-T. Wu, Light: Sci. Appl. **6**, e17043 (2017).
11. K. Qasim, B. Wang, Y. Zhang, P. Li, Y. Wang, S. Li, S. Lee, L. Liao, W. Lei, and Q. Bao, Adv. Funct. Mater. **27**, 1606874 (2017).
12. M. G. Helander, Z.-B. Wang, M. T. Greiner, Z.-W. Liu, J. Qiu, and Z.-H. Lu, Adv. Mater. **22**, 2037 (2010).
13. S. Schubert, M. Hermenau, J. Meiss, L. Müller-Meskamp, and K. Leo, Adv. Funct. Mater. **22**, 4993 (2012).
14. Y. Xia, K. Sun, and J. Ouyang, Adv. Mater. **24**, 2436 (2012).
15. D. Gupta, M. M. Wienk, and R. A. J. Janssen, Adv. Energy Mater. **3**, 782 (2013).
16. P.-C. Hsu, S. Wang, H. Wu, V. K. Narasimhan, D. Kong, H. Ryoung Lee, and Y. Cui, Nat. Commun. **4**, 2522 (2013).
17. J. Lee, S. T. Connor, Y. Cui, and P. Peumans, Nano Lett. **8**, 689 (2008).
18. Y.-G. Bi, J. Feng, Y.-F. Li, Y.-L. Zhang, Y.-S. Liu, L. Chen, Y.-F. Liu, L. Guo, S. Wei, and H.-B. Sun, ACS Photon. **1**, 690 (2014).
19. P. You, Z. Liu, Q. Tai, S. Liu, and F. Yan, Adv. Mater. **27**, 3632 (2015).
20. V. Apalkov and M. I. Stockman, Light: Sci. Appl. **3**, e191 (2014).
21. M. Xu, J. Feng, Z.-J. Fan, X.-L. Ou, Z.-Y. Zhang, H.-Y. Wang, and H.-B. Sun, Solar Energy Mater. Sol. Cells **169**, 8 (2017).
22. X.-L. Ou, J. Feng, M. Xu, and H.-B. Sun, Opt. Lett. **42**, 1958 (2017).
23. X.-L. Ou, M. Xu, J. Feng, and H.-B. Sun, Solar Energy Mater. Sol. Cells **157**, 660 (2016).
24. T.-H. Han, M.-R. Choi, S.-H. Woo, S.-Y. Min, C.-L. Lee, and T.-W. Lee, Adv. Mater. **24**, 1487 (2012).
25. R. A. Hatton, M. R. Willis, M. A. Chesters, and D. Briggs, J. Mater. Chem. **13**, 722 (2003).
26. Y.-G. Bi, J. Feng, J.-H. Ji, Y. Chen, Y.-S. Liu, Y.-F. Li, Y.-F. Liu, X.-L. Zhang, and H.-B. Sun, Nanoscale **8**, 10010 (2016).
27. Y.-S. Liu, J. Feng, X.-L. Ou, H.-F. Cui, M. Xu, and H.-B. Sun, Org. Electron. **31**, 247 (2016).
28. Y.-F. Liu, M.-H. An, Y.-G. Bi, D. Yin, J. Feng, and H.-B. Sun, IEEE Photon. J. **9**, 7000606 (2017).
29. G. Niu, X. Guo, and L. Wang, J. Mater. Chem. **3**, 8970 (2015).